Vertex corrections due to the triangle singularity mechanism in the light axial vector meson couplings to $K^*\bar{K}+\text{c.c.}$

Meng-Chuan Du,[*] Yin Cheng,[†] and Qiang Zhao[‡]

Institute of High Energy Physics, Chinese Academy of Sciences, Beijing 100049, China
and University of Chinese Academy of Sciences, Beijing 100049, China

(Received 10 June 2022; accepted 23 August 2022; published 16 September 2022)

The light axial vector mesons can couple to $K^*\bar{K}+\text{c.c.}$ in an S wave at the tree level. Because of the near-threshold S-wave interactions, the couplings can be affected by the final state interactions. It is of peculiar interest that the pion exchange between $K^*\bar{K}+\text{c.c.}$ can go through a triangle diagram which is within the kinematics of the triangle singularity. This mechanism will introduce energy dependence and a D-wave amplitude to the vertex couplings. Hence, it should be necessary to investigate the role played by the $K^*\bar{K}+\text{c.c.}$ threshold in order to have a better understanding of the light axial vector spectrum.

DOI: 10.1103/PhysRevD.106.054019

I. INTRODUCTION

In the constituent quark model, the light axial vector mesons are categorized as P-wave quark and antiquark systems with $J^{PC}=1^{+(+)}$ and $1^{+(-)}$, while the positive and negative charge conjugate parities indicate the total spins of the quark and antiquark systems to be either parallel or antiparallel. Although the light flavor SU(3) nonets for these two axial vectors have been established in experiment [1], it seems that our knowledge about these structures is still far from satisfactory.

In the Particle Data Group (PDG) [1], the assignments of the nonstrange multiplets are $f_1(1285)$, $f_1(1420)$, and $a_1(1260)$ for the 1^{++} sector and $h_1(1170)$, $h_1(1415)$, and $b_1(1235)$ for the 1^{+-} sector. The strange multiplets can mix with each other and form $K_1(1270)$ and $K_1(1400)$ as their mass eigenstates. Although there have been a lot of theoretical and experimental studies on these states, there are still some puzzling issues about their nature and decays. In particular, the open $K^*\bar{K}$ threshold phenomenon is relevant. In Ref. [2], a unitary isobar model was constructed to describe the three-body interaction of the $K\bar{K}\pi$ system, where $f_1(1420)$ can be described as a $K\bar{K}\pi$ molecule. In Ref. [3], the axial vector mesons were studied with SU(3) chiral Lagrangians for the vector-pseudoscalar meson scatterings as dynamically generated states. Given the large S-wave couplings to the $K^*\bar{K}+\text{c.c.}$, channel pole structures, which can be identified as the physical states $h_1(1380)$, $f_1(1285)$, and $b_1(1235)$, were seen in the scattering amplitudes. In Ref. [4], with a Weinberg-Tomozawa term for the vector-pseudoscalar scattering, poles corresponding to $f_1(1285)$, $a_1(1260)$, $h_1(1170)$, $h_1(1415)$, $b_1(1235)$, and $K_1(1270)$ were found on the second Riemann sheet of scattering amplitudes, which agreed with Ref. [3] and suggested a molecular nature of these states. Moreover, the analysis of Ref. [4] showed that $f_1(1420)$ and $K_1(1400)$ were unlikely to be accommodated by the molecular picture. In several follow-up studies [5–13], a common result was reached that $f_1(1285)$ was consistent to be a $K^*\bar{K}+\text{c.c.}$ hadronic molecular state due to its strong S-wave couplings to the $K^*\bar{K}+\text{c.c.}$ channel. In contrast, $f_1(1420)$ cannot be accommodated by the molecular picture. A new interpretation of $f_1(1420)$ was triggered later by the recognition of contributions from the triangle singularity (TS) mechanism in the $K^*\bar{K}+\text{c.c.}$ scatterings into $\eta\pi\pi$ or $K\bar{K}\pi$ in the f_1 decays.

The TS mechanism is a peculiar threshold phenomenon which was first identified by Landau [14] in the final state rescatterings with a t-channel particle exchange to form a triangle loop. It occurs in such a kinematic region where all the internal particles of the triangle loop can be simultaneously on shell and can result in a characteristic logarithmic singularity for the loop transition amplitude. Although this phenomenon was predicted a long time ago, its effect was not observed until quite recently. In Ref. [15], the TS effects due to the $K^*\bar{K}+\text{c.c.}$ rescattering by exchanging a kaon were proposed to explain the large isospin violation in $J/\psi\to\gamma\eta(1405/1475)\to\gamma+3\pi$ [16]. In the follow-up extensive studies [17–21], the detailed analyses including possible mechanisms have provided

[*]dumc@ihep.ac.cn
[†]chengyin@ihep.ac.cn
[‡]zhaoq@ihep.ac.cn

crucial information for understanding the pseudoscalar states $\eta(1405/1475)$. In Ref. [17], it is shown that the angular distribution of the π recoiling against $f_0(980)$ in $J/\psi \to \gamma + 3\pi$ requires the $f_1(1420)$ contribution, where the open S-wave $K^*\bar{K}$ threshold effect via the TS mechanism is important. Besides, the TS mechanism also provides a natural explanation to the $a_1(1420)$ observed in the $f_0(980)\pi$ final state in $\pi^- p$ scattering [22–25] observed by the COMPASS Collaboration [26]. Recent studies of the manifestations of the TS mechanism can be found in Ref. [22] and recent reviews of Refs. [27,28].

It was proposed by Ref. [9] that $f_1(1420)$ should not be a genuine state, but a kinematic effect of the TS mechanism in the decay of $f_1(1285)$. It is argued in Ref. [9] that the TS affects only the $f_1(1285) \to a_0(980)\pi$ decay. The $K^*\bar{K} + \text{c.c.}$ decay is the normal decay of $f_1(1285) \to K\bar{K}\pi$. When the initial energy increases, the TS due to the $f_1(1285)$ will produce a peak of $f_1(1420)$ at 1420 MeV. In the $\eta\pi\pi$ decay channel, the line shape of the spectrum based on this scenario is indeed consistent with the WA102 observation [29]. However, in the $K\bar{K}\pi$ channel, the calculation of Ref. [9] gives a flat and wide enhancement near the mass of $f_1(1420)$, which is inconsistent with the strongly enhanced sharp peaks observed in various measurements [30–33]. This suggests that the TS mechanism due to $f_1(1285)$ decays is not strong enough to account for the large cross sections for the production of $f_1(1420)$.

In order to disentangle the role played by the TS mechanism, the production of the light axial vector partial wave contributions was investigated by Ref. [34] in J/ψ decay. The TS effect followed by the $K^*\bar{K}$ open S-wave channel with $J^{PC} = 1^{+-}$ is studied in Ref. [34], where the pole contributions are not included. In Ref. [23], a comprehensive study on light axial vector mesons is presented by assuming all these axial states are the genuine quark-model states but affected by the TS. The couplings between the axial vectors (i.e., 1^{++} and 1^{+-} states) and $K^*\bar{K} + \text{c.c.}$ are assumed to be energy independent and symmetric under the SU(3) flavor group. This assumption needs further investigation, since the pion exchange between K^* and $\bar{K}$ can renormalize the axial vector meson couplings to the $K^*\bar{K} + \text{c.c.}$ channel. Nevertheless, since the exchanged pion can be on shell, the occurrence of the TS may cause highly nontrivial effects. This motivates us to investigate the axial vector meson couplings to $K^*\bar{K} + \text{c.c.}$ dressed by the TS mechanism, and it should provide further information for our understanding of the nature of these axial vector states.

In Sec. II, we will define the axial vector meson couplings to $K^*\bar{K} + \text{c.c.}$ and provide the formalism of the transition amplitudes with the triangle loop corrections. In Sec. III, we will present the numerical results and discuss the impact of the triangle loop corrections on the vertex couplings. Conclusions will be made in the last section.

II. AXIAL VECTOR MESON COUPLINGS TO $K^*\bar{K} + \text{c.c.}$

A. Tree-level couplings

The nonstrange light axial vector mesons $f_1(1420)$ and $h_1(1415)$ can couple to $K^*\bar{K}$ in an S wave and then decay into $K\bar{K}\pi$. In this work, we focus on the these two states, since their masses are within the TS kinematic region. We mention in advance that the TS corrections to the couplings between the lower mass states, i.e. $f_1(1285)$, $a_1(1260)$, $h_1(1170)$, $b_1(1235)$, and $K^*\bar{K}$ are small and can be neglected. Meanwhile, the $a_1(1420)$ can be regarded as a nonresonance structure caused by the TS.

In Fig. 1, the tree-level processes for $A \to K^*\bar{K} + \text{c.c.} \to K^0\bar{K}^0\pi$ are illustrated, where A represents the nonstrange axial vector states f_1 with $J^{PC} = 1^{++}$ or h_1 with $J^{PC} = 1^{+-}$, respectively. A bare interaction between A and $K^*\bar{K} + \text{c.c.}$ respecting the SU(3) flavor symmetry is introduced in Fig. 1, i.e.,

$$\begin{aligned} L_{f_1VP} &= g_{f_1VP}\langle f_1^\mu [V_\mu, P]\rangle, \\ L_{h_1VP} &= i g_{h_1VP}\langle h_1^\mu \{V_\mu, P\}\rangle, \end{aligned} \tag{1}$$

where $\langle \ldots \rangle$ represents the trace of the matrix inside and V and P are the vector and pseudoscalar meson fields, respectively; g_{f_1VP} and g_{h_1VP} are the corresponding coupling constants. The transition of $K^* \to K\pi$ is described by

$$L_{VPP} = i g_{VPP}\langle V^\mu [\partial_\mu P, P]\rangle, \tag{2}$$

with $g_{VPP} = 4.52$ calculated by the $\phi \to K\bar{K}$ or $K^* \to K\pi$ decays. The SU(3) multiplets of the vector and pseudoscalar mesons are given, respectively, as follows:

$$V^\mu \equiv \begin{pmatrix} \frac{\rho^0}{\sqrt{2}} + \frac{\omega}{\sqrt{2}} & \rho^+ & K^{*+} \\ \rho^- & \frac{-\rho^0}{\sqrt{2}} + \frac{\omega}{\sqrt{2}} & K^{*0} \\ K^{*-} & \bar{K}^{*0} & \phi \end{pmatrix} \tag{3}$$

and

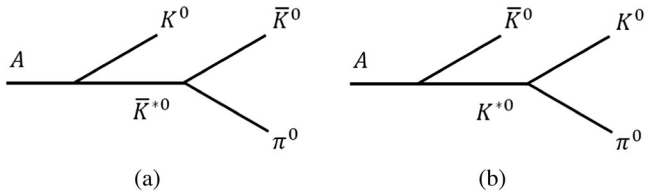

FIG. 1. (a,b) Tree-level transitions of $A \to K^0\bar{K}^0\pi^0$, where $A = f_1$ or h_1 are implied.

$$P \equiv \begin{pmatrix} \frac{\pi^0}{\sqrt{2}} + \frac{\cos\alpha_P\eta + \sin\alpha_P\eta'}{\sqrt{2}} & \pi^+ & K^+ \\ \pi^- & -\frac{\pi^0}{\sqrt{2}} + \frac{\cos\alpha_P\eta + \sin\alpha_P\eta'}{\sqrt{2}} & K^0 \\ K^- & \bar{K}^0 & -\sin\alpha_P\eta + \cos\alpha_P\eta' \end{pmatrix}, \tag{4}$$

where the mixing between η and η' is defined as

$$\begin{pmatrix} \eta \\ \eta' \end{pmatrix} = \begin{pmatrix} \cos\alpha_P & -\sin\alpha_P \\ \sin\alpha_P & \cos\alpha_P \end{pmatrix} \begin{pmatrix} \eta_n \\ \eta_s \end{pmatrix}, \tag{5}$$

with $\eta_n \equiv (u\bar{u} + d\bar{d})/\sqrt{2}$ and $\eta_s \equiv s\bar{s}$, and α_P is the mixing angle.

The tree-level amplitudes in Figs. 1(a) and 1(b) can be obtained:

$$\begin{aligned} M_1^{\rm tree} &= g_{\rm tree1}\epsilon_\mu \frac{i\left(-g_{\mu\nu} + \frac{(p_b+p_d)_\mu (p_b+p_d)_\nu}{s_{bd}}\right)}{s_{bd} - m_{K^*}^2 + i m_{K^*}\Gamma_{K^*}} i(p_b - p_d)^\nu \\ &= -\frac{1}{s_{bd} - m_{K^*}^2 + i m_{K^*}\Gamma_{K^*}} g_{\rm tree1}\epsilon_\mu \left[\left(-1 + \frac{s_b - s_d}{s_{bd}}\right)p_b^\mu + \left(1 + \frac{s_b - s_d}{s_{bd}}\right)p_d^\mu\right], \end{aligned} \tag{6}$$

$$\begin{aligned} M_2^{\rm tree} &= g_{\rm tree2}\epsilon_\mu \frac{i\left(-g_{\mu\nu} + \frac{(p_a+p_d)_\mu (p_a+p_d)_\nu}{s_{ad}}\right)}{s_{ad} - m_{K^*}^2 + i m_{K^*}\Gamma_{K^*}} i(p_a - p_d)^\nu \\ &= -\frac{1}{s_{ad} - m_{K^*}^2 + i m_{K^*}\Gamma_{K^*}} g_{\rm tree2}\epsilon_\mu \left[\left(-1 + \frac{s_a - s_d}{s_{ad}}\right)p_a^\mu + \left(1 + \frac{s_a - s_d}{s_{ad}}\right)p_d^\mu\right], \end{aligned} \tag{7}$$

where the momenta of $\bar{K}^0$, K^0, and π^0 are labeled by p_a, p_b, and p_d, respectively. The invariant masses squared of the $K^0\pi$ and $\bar{K}^0\pi$ subsystem are denoted by $s_{ad} = (p_a + p_d)^2 \equiv p_c^2$ and $s_{bd} = (p_b + p_d)^2$, respectively, and a constant width for the K^* meson is adopted, i.e., $\Gamma_{K^*} = 50$ MeV. The products of coupling constants in Figs. 1(a) and 1(b) are grouped into $g_{\rm tree1}$ and $g_{\rm tree2}$, respectively. For instance, for the initial state A ($A = f_1$ or h_1), we define

$$g_{\rm tree1} \equiv i\frac{1}{\sqrt{2}} g_{AK^{*0}\bar{K}^0} g_{VPP}, \tag{8}$$

$$g_{\rm tree2} \equiv -i\frac{1}{\sqrt{2}} g_{A\bar{K}^{*0}K^0} g_{VPP}. \tag{9}$$

Note that for the $C = +1$ state, e.g., $f_1(1420)$, one has $g_{\rm tree1} = g_{\rm tree2}$, but for the $C = -1$ state, e.g., $h_1(1415)$, a sign should be included, i.e., $g_{\rm tree1} = -g_{\rm tree2}$. Since the axial vector states with $C = \pm 1$ can decay into the same $K\bar{K}\pi$ final state, the interference effect can manifest itself at the intersection of the K^* and $\bar{K}^*$ resonance bands in the Dalitz plot.

B. Triangle loop corrections

As mentioned earlier, the S-wave coupling in Eq. (1) is subject to dressing by the π exchange between the intermediate K^* and $\bar{K}$ mesons. As shown in Fig. 2, the triangle diagrams can contribute to the couplings of the axial vector mesons to $K^*\bar{K}$ + c.c.. Taking into account that the transition processes in Fig. 2 satisfy the TS condition, it is interesting to find out how important the triangle loop correction is and how it should affect the line shapes in the invariant mass spectra.

With the interactions given in Eqs. (1) and (2), the amplitudes in Fig. 2 read

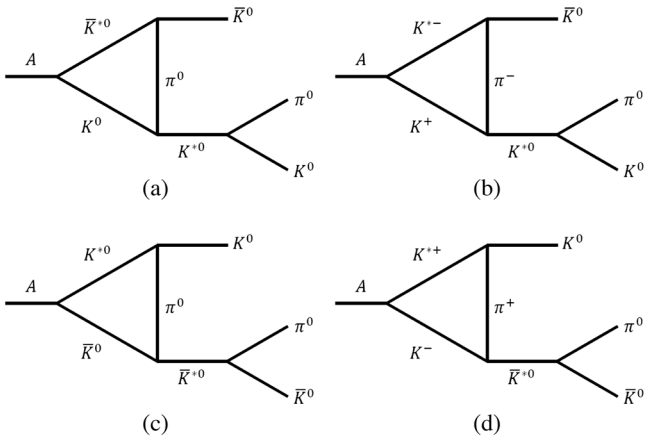

FIG. 2. (a–d) Triangle diagrams of $A \to K^0\bar{K}^0\pi^0$ through π exchange.

$$M_a^{\rm tri} = \epsilon_\mu I_a^{\mu\alpha} \frac{i(-g_{\alpha\beta} + \frac{(p_b+p_d)_\alpha (p_b+p_d)_\beta}{s_{bd}})}{s_{bd} - m_{K^*}^2 + i m_{K^*}\Gamma_{K^*}} i(p_b - p_d)^\beta g_a, \quad (10)$$

$$M_b^{\rm tri} = \epsilon_\mu I_b^{\mu\alpha} \frac{i(-g_{\alpha\beta} + \frac{(p_b+p_d)_\alpha (p_b+p_d)_\beta}{s_{bd}})}{s_{bd} - m_{K^*}^2 + i m_{K^*}\Gamma_{K^*}} i(p_b - p_d)^\beta g_b, \quad (11)$$

$$M_c^{\rm tri} = \epsilon_\mu I_c^{\mu\alpha} \frac{i(-g_{\alpha\beta} + \frac{(p_a+p_d)_\alpha (p_a+p_d)_\beta}{s_{ad}})}{s_{ad} - m_{K^*}^2 + i m_{K^*}\Gamma_{K^*}} i(p_a - p_d)^\beta g_c, \quad (12)$$

$$M_d^{\rm tri} = \epsilon_\mu I_d^{\mu\alpha} \frac{i(-g_{\alpha\beta} + \frac{(p_a+p_d)_\alpha (p_a+p_d)_\beta}{s_{ad}})}{s_{ad} - m_{K^*}^2 + i m_{K^*}\Gamma_{K^*}} i(p_a - p_d)^\beta g_d, \quad (13)$$

where the subscripts denote the corresponding processes in Fig. 2.

In each diagram, the couplings from all vertices are grouped into $g_{a,b,c,d}$, i.e.,

$$g_a = \frac{1}{\sqrt{2}} g_b = \frac{i}{2\sqrt{2}} g_{A\bar{K}^{*0}K^0} g_{VPP}^3, \quad (14)$$

$$g_c = \frac{1}{\sqrt{2}} g_d = -\frac{i}{2\sqrt{2}} g_{AK^{*0}\bar{K}^0} g_{VPP}^3. \quad (15)$$

For the initial state with $C = +1$, $g_a = g_c$, while for $C = -1$, $g_a = -g_c$. The tensor loop integral is defined by

$$\begin{aligned} I_{c,d}^{\mu\alpha} &= \int \frac{d^4q}{(2\pi)^4} \frac{i^3(-g^{\mu\nu} + \frac{q^\mu q^\nu}{q^2}) i(2p_b - q)_\nu (-i)(p_c + 2p_b - 2q)^\alpha \mathcal{F}(q^2)}{(q^2 - m_1^2)[(q-p_b)^2 - m_2^2][(q - p_b - p_c)^2 - m_3^2]} \\ &= -i[\Lambda_0(s_0, s_b, s_{ad}) g^{\mu\alpha} + \Lambda_{cb}(s_0, s_b, s_{ad}) p_c^\mu p_b^\alpha + \Lambda_{bb}(s_0, s_b, s_{ad}) p_b^\mu p_b^\alpha] \end{aligned} \quad (16)$$

and

$$\begin{aligned} I_{a,b}^{\mu\alpha} &= I_{c,d}^{\mu\alpha}|_{p_b \to p_a, p_a \to p_b} \\ &= -i[\Lambda_0(s_0, s_a, s_{bd}) g^{\mu\alpha} + \Lambda_{cb}(s_0, s_a, s_{bd})(p_b + p_d)^\mu p_a^\alpha + \Lambda_{bb}(s_0, s_a, s_{bd}) p_a^\mu p_a^\alpha], \end{aligned} \quad (17)$$

where $\mathcal{F}(q^2)$ is a monopole form factor to regularize the divergence of the loop integrals, i.e.,

$$\mathcal{F}(q^2) = \prod_{i=1}^{3} \frac{m_i^2 - \Lambda_i^2}{q_i^2 - \Lambda_i^2}, \quad (18)$$

with q_i the momenta of internal lines as functions of q and $\Lambda_i \equiv m_i + \beta\Lambda_{\rm QCD}$. In the numerical calculations, $\Lambda_{\rm QCD} = 250$ MeV and $\beta = 2$ are adopted.

In Eqs. (16) and (17), the Lorentz scalars Λ_0, Λ_{cb}, and Λ_{bb} are parametrized out. There are some typical features of the tensor integral $I^{\mu\alpha}$.

(i) $I^{\mu\alpha}$ contracts ϵ_μ and $\epsilon_{K^*\alpha}^*$. The $g^{\mu\alpha}$ term in Eqs. (16) and (17) leads to $\epsilon \cdot \epsilon_{K^*}^*$, so that it is a leading-order correction to the bare tree-level S-wave interaction. The bare coupling $g_{AK^*\bar{K}}$ will receive a loop correction from Λ_0, which will change both the absolute value and the phase of $g_{AK^*\bar{K}}$. The physical S-wave $A \to K^*\bar{K}$ coupling $g^{\rm eff}$ becomes

$$g_{AK^{*0}\bar{K}^0}^{\rm eff} = g_{AK^{*0}\bar{K}^0} + g_a' \Lambda_{0a} + g_b' \Lambda_{0b}, \quad (19)$$

$$g_{A\bar{K}^{*0}K^0}^{\rm eff} = g_{A\bar{K}^{*0}K^0} + g_c' \Lambda_{0c} + g_d' \Lambda_{0d}, \quad (20)$$

where the subscripts a, b, c, and d are used to distinguish the different internal mass configurations in Fig. 2. The couplings are

$$g_a' = \frac{1}{\sqrt{2}} g_b' = \frac{i}{2} g_{A\bar{K}^{*0}K^0} g_{VPP}^2, \quad (21)$$

$$g_c' = \frac{1}{\sqrt{2}} g_d' = \frac{i}{2} g_{AK^{*0}\bar{K}^0} g_{VPP}^2. \quad (22)$$

(ii) The other two terms in $I^{\mu\alpha}$ are equivalent to a D-wave interaction between the axial vector A and $K^*\bar{K}$ + c.c. and will give rise to different distribution in the Dalitz plot of the $K\bar{K}\pi$ final state.

(iii) The $g^{\mu\alpha}$ term also receives a D-wave contribution to the $K^*\bar{K}$ coupling. As a consequence, the $g^{\mu\alpha}$ term will interfere with the remaining two terms, even after the whole phase space integration.

To unambiguously define the S- and D-wave parts of $I^{\mu\alpha}$, one has to separate out the pure S-wave amplitude in Λ_0, which does not interfere with the remaining terms when the whole amplitude is squared. This separation is unique. For $I_{cd}^{\mu\alpha}$, the S- and D-wave parts read, respectively,

$$I_S^{\mu\alpha} = -i\left(\Lambda_0 - \frac{\sqrt{s}E_c}{1 + \frac{3s_{ad}}{|\vec{p}_c|^2}}(\Lambda_{bb} - \Lambda_{cb})\right) g^{\mu\alpha} \quad (23)$$

and

$$I_D^{\mu\alpha} = -i\frac{\sqrt{s}E_c}{1 + \frac{3s_{ad}}{|\vec{p}_c|^2}}(\Lambda_{bb} - \Lambda_{cb}) g^{\mu\alpha} - i(\Lambda_{cb} p_c^\mu p_b^\alpha + \Lambda_{bb} p_b^\mu p_b^\alpha), \quad (24)$$

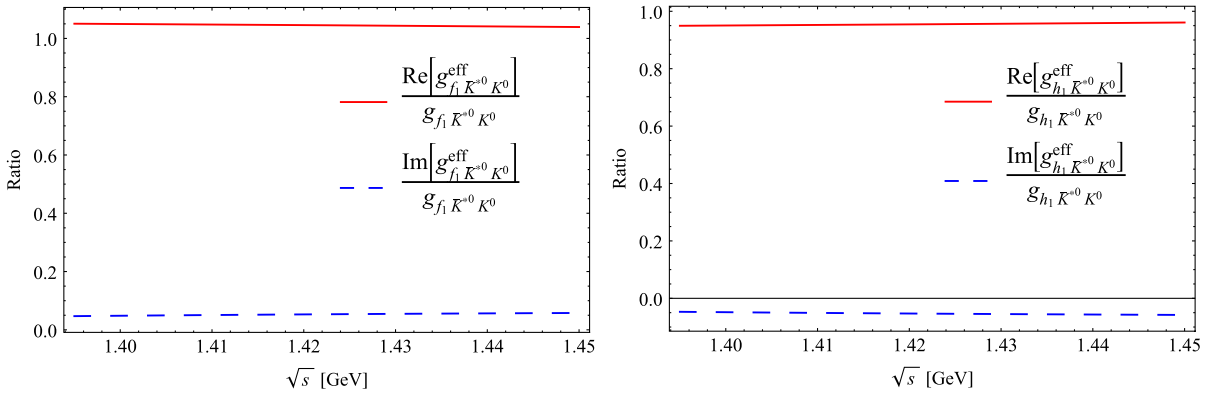

FIG. 3. The dressed S-wave coupling $\mathrm{Re}[g^{\mathrm{eff}}_{A(B)\bar{K}^{*0}K^0}]/g_{A(B)\bar{K}^{*0}K^0}$ (red solid lines) and $\mathrm{Im}[g^{\mathrm{eff}}_{A(B)\bar{K}^{*0}K^0}]/g_{A(B)\bar{K}^{*0}K^0}$ (blue dashed lines) for $f_1(1420) \to \bar{K}^{*0}K^0$ (left) and $h_1(1415) \to \bar{K}^{*0}K^0$ (right).

where E_c and $\vec{p}_c$ are, respectively, the energy and 3-momentum of $\bar{K}^*$ in the rest frame of the initial state. With Eqs. (23) and (24), we are able to define the pure S- and D-wave amplitudes M_S and M_D, similar to Eqs. (10)–(13). It can be immediately seen from Eqs. (23) and (24) that the new term proportional to $|\vec{p}_c|^2$ is suppressed near threshold, which is indeed typical behavior of a D-wave coupling. This is consistent with the effects of higher-order chiral kernels studied in Ref. [5].

For the two-body decay $A \to K^*\bar{K}$, it can be proved that the functions $I^{\mu\alpha}_S$ and $I^{\mu\alpha}_D$ do not interfere. For the three-body decay $A \to K^*\bar{K} + \mathrm{c.c.} \to K\bar{K}\pi$, there are contributions from two intermediate charge-conjugate channels, i.e., $K^*\bar{K}$ and $\bar{K}^*K$. For every single channel, e.g., $K^*\bar{K}$, the terms of $I^{\mu\alpha}_S$ and $I^{\mu\alpha}_D$ do not interfere after the phase space integration over the invariant mass of $\bar{K}\pi$. However, the term of $I^{\mu\alpha}_S$ of one channel may interfere with $I^{\mu\alpha}_D$ of the other channel, even though the phase space integration is performed.

The full amplitude for $A \to K^*\bar{K} + \mathrm{c.c.} \to K^0\bar{K}^0\pi^0$ reads

$$M^{\mathrm{full}}_{A\to K^*\bar{K}+\mathrm{c.c.}\to K^0\bar{K}^0\pi^0} = \sum_{i=a,b,c,d} M^{\mathrm{tri}}_i + \sum_{i=1,2} M^{\mathrm{tree}}_i. \quad (25)$$

III. RESULTS AND DISCUSSION

In this section, we present the numerical results for $A \to K\bar{K}\pi$ with $A = f_1(1420)$ or $h_1(1415)$. We first examine the TS effects on the coupling constants and then investigate the TS interfering effects on the line shapes.

Actually, for the pure S-wave tree-level couplings, the triangle diagrams will result in corrections to the S-wave coupling constants and introduce a small D-wave contribution to the vertex. The bare S-wave coupling $g_{AK^*\bar{K}}$ will be shifted to the physical S-wave coupling $g^{\mathrm{eff}}_{AK^*\bar{K}}$, and, because of the loop function, $g^{\mathrm{eff}}_{AK^*\bar{K}}$ is, in general, a complex number. For the on-shell K^* meson, we evaluate the relative ratios $\mathrm{Re}[g^{\mathrm{eff}}_{AK^*\bar{K}}]/g_{AK^*\bar{K}}$ and $\mathrm{Im}[g^{\mathrm{eff}}_{AK^*\bar{K}}]/g_{AK^*\bar{K}}$, for $f_1(1420)$ and $h_1(1415)$, and the results are presented in Fig. 3. It shows that the TS indeed brings non-negligible corrections to the axial vector couplings to $K^*\bar{K} + \mathrm{c.c.}$ which are at the order of 5%. It also introduces different phases to the physical couplings.

The vertex corrections will result in corrections to the tree-level partial decay width Γ for $A \to K\bar{K}\pi$, which is calculated by the tree-level amplitudes [Eqs. (6) and (7)]. We define $\delta\Gamma \equiv \Gamma' - \Gamma$, where Γ' is the corrected partial width calculated by Eq. (25). Then, the ratio $\delta\Gamma/\Gamma$ will measure the loop correction effects at the physical mass. With the regularization parameter $\beta = 2$, we obtain

$$\frac{\delta\Gamma(f_1(1420) \to K^*\bar{K} \to K\bar{K}\pi)}{\Gamma(f_1(1420) \to K^*\bar{K} \to K\bar{K}\pi)} = 15\%, \quad (26)$$

$$\frac{\delta\Gamma(h_1(1415) \to K^*\bar{K} \to K\bar{K}\pi)}{\Gamma(h_1(1415) \to K^*\bar{K} \to K\bar{K}\pi)} = -9.3\%. \quad (27)$$

It should be stressed that the triangle diagrams contain both S- and D-wave amplitudes, and Γ' is calculated taking into account both contributions. The ratios indicate non-negligible effects arising from the vertex corrections. It shows that inclusions of the vertex correction and the TS effects should be necessary in the partial wave analysis of $A \to K\bar{K}\pi$.

In Fig. 4, the $\bar{K}\pi$ spectra of $f_1(1420) \to K^*\bar{K} + \mathrm{c.c.} \to K\bar{K}\pi$ and $h_1(1415) \to K^*\bar{K} + \mathrm{c.c.} \to K\bar{K}\pi$ at their physical masses are shown in the left and right panel, respectively. The vertex corrections and triangle loop contributions produce nontrivial spectra. The tree diagrams turn out to be dominant where the $\bar{K}^*$ peaks can be identified. Apart from the $\bar{K}^*$ peaks in both cases, the lower broad bumps are the kinematic reflections from the $K^* \to K\pi$ channel which recoils $\bar{K}$ at the K^* mass. It shows that the correction to the partial width is at the order of 10%.

Note that, although we calculate the vertex coupling corrections to the axial vector meson couplings to $K^*\bar{K} + \mathrm{c.c.}$, we actually show the spectra of the three-body decay channel $K\bar{K}\pi$ via the intermediate $K^*\bar{K} + \mathrm{c.c.}$.

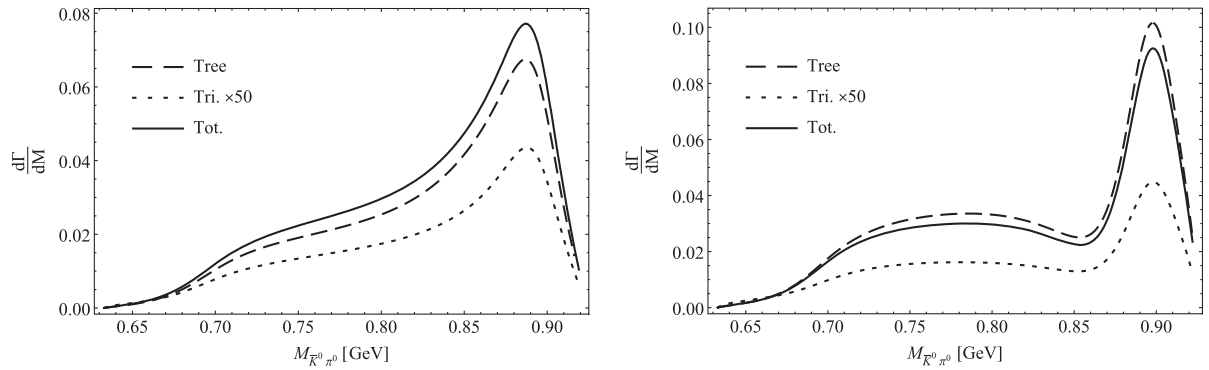

FIG. 4. The $\bar{K}\pi$ spectra for $f_1(1420) \to K^*\bar{K} + \text{c.c.} \to K\bar{K}\pi$ (left) and $h_1(1415) \to K^*\bar{K} + \text{c.c.} \to K\bar{K}\pi$ (right). The solid, dashed, and dotted lines represent the total, tree, and triangle (intensified by 50) contributions, respectively.

This is due to the consideration that the interference of the TS may cause changes to the K^* line shape. In fact, the dominance of the tree diagrams and the width effects of the intermediate K^* has smoothed the TS structures produced by the charged and neutral $\bar{K}\pi$ thresholds in the invariant mass spectrum of $\bar{K}^0\pi^0$.

We also mention that for the final state of $K\bar{K}\pi$ other processes, such as $a_0\pi$ and $\kappa\bar{K} + \text{c.c.}$, may contribute in addition to the intermediate $K^*\bar{K} + \text{c.c.}$ transition. It means a combined analysis should be necessary in the future with the available data.

Qualitatively, the correction affects the line shape of the two-body spectra rather weakly but should not be neglected. Nevertheless, the vertex corrections will introduce a D-wave amplitude in $I^{\mu\alpha}$. To quantify the contribution from the D-wave part in $I^{\mu\nu}$, we illustrate the individual contributions from the pure S-wave (dashed line) and pure D-wave (dotted lines) parts in Fig. 5. In both cases for the $f_1(1420)$ and $h_1(1415)$ decays, the D-wave amplitude is significantly smaller than the tree-level S-wave one, which suggests that the loop corrections will not alter the line shapes of $K\pi$ spectra in Fig. 4. This also means that the vertex corrections do not cause significant changes to the line shapes and a leading-order calculation based on the tree-level S-wave couplings is reasonable in the description of the $K\pi$ (or $\bar{K}\pi$) line shapes from the intermediate $K^*\bar{K} +$ c.c. rescatterings [23].

The dominance of the TS mechanism in the vertex corrections suggests that the main contributions of the triangle loops should come from the kinematic region where these internal particles are nearly on shell. It allows one to make a nonrelativistic expansion to the numerator of Eq. (16) by the substitution of $-g^{\mu\nu} + \frac{q^\mu q^\nu}{q^2} \to \delta^{\mu\nu} = -g^{\mu\nu} + g^{0\mu}g^{0\nu}$. In this way, the numerator of the integrand in Eq. (16) becomes

$$num \to 4p_b^\mu p_b^\alpha - 4p_b^\mu q^\alpha - 2q^\mu p_b^\alpha + 2q^\mu q^\alpha, \quad (28)$$

where the only term leading to the three-point scalar loop integral C_0 is from $4p_b^\mu p_b^\alpha$. However, one notices that this is a D-wave term and proportional to $|\vec{p}_c|^2$. Thus, the amplitude is actually suppressed in the kinematic region near threshold. This explains why the TS effects do not produce significant vertex corrections to the coupling in both S and D waves. In Fig. 6, the results for the $\bar{K}\pi$ invariant mass spectra with the relativistic and nonrelativistic amplitudes of the triangle diagrams are compared.

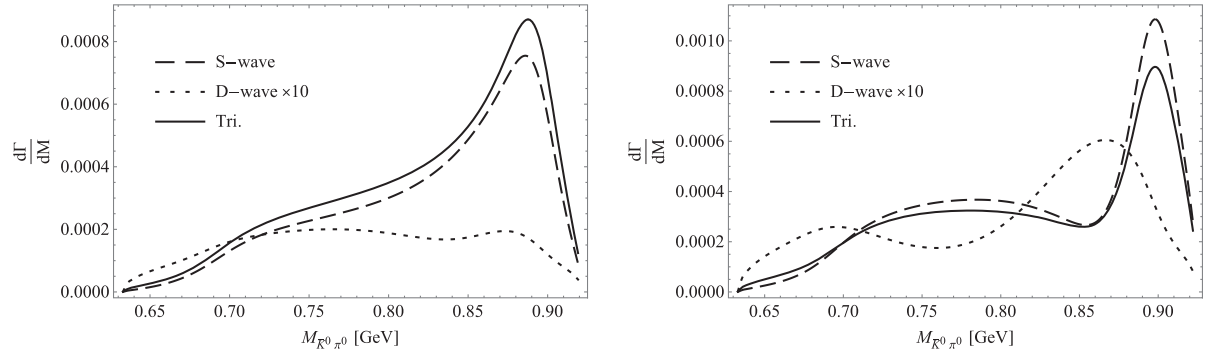

FIG. 5. The $\bar{K}\pi$ spectra for $f_1(1420) \to K^*\bar{K} + \text{c.c.} \to K\bar{K}\pi$ (left) and $h_1(1415) \to K^*\bar{K} + \text{c.c.} \to K\bar{K}\pi$ (right) from the triangle loops. The solid lines are full triangle amplitudes. The dashed lines denote the pure S-wave contributions from the loop amplitudes, while the dotted lines are the pure D-wave contributions multiplied by a factor of 10.

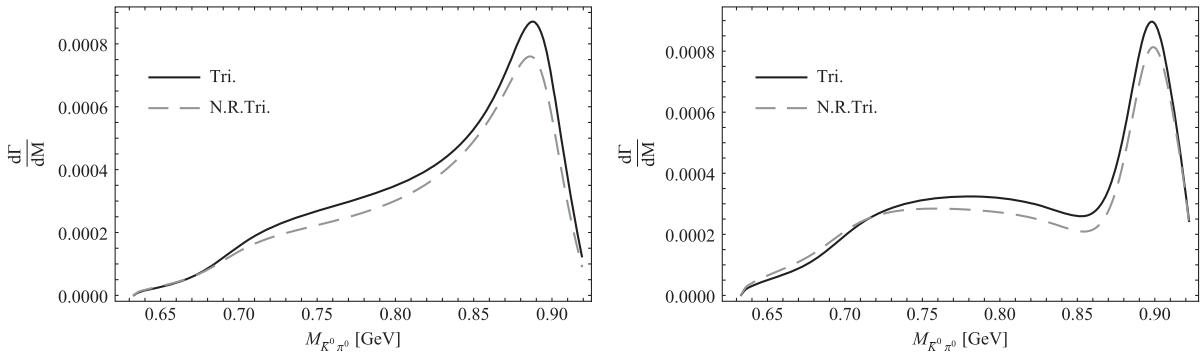

FIG. 6. The $\bar{K}\pi$ spectra for $f_1(1420) \to K^*\bar{K} + \text{c.c.} \to K\bar{K}\pi$ (left) and $h_1(1415) \to K^*\bar{K} + \text{c.c.} \to K\bar{K}\pi$ (right) from triangle loops. The solid and dashed lines are calculation results based on the relativistic and nonrelativistic formalism, respectively.

The difference indicates the effects of the nonrelativistic expansion. One sees that these two results agree with each other quite well.

It is interesting to mention that the triangle loops considered here, namely, $K^*\bar{K}(\pi) + \text{c.c.}$, are relatively suppressed in comparison with the ones involving $K^*\bar{K}(K) + \text{c.c.}$ such as $h_1(1415) \to \phi\pi$ [23]. For the latter cases, the TS contributions are relatively enhanced by the larger phase spaces.

IV. CONCLUSION

We investigate the triangle loop corrections to the axial vector couplings to $K^*\bar{K} + \text{c.c.}$ where the TS mechanism can contribute. Because of the triangle loop transitions, the tree-level S-wave couplings for $f_1(1420)$ and $h_1(1415)$ to $K^*\bar{K} + \text{c.c.}$ will be corrected by about 5%, and a D-wave coupling can arise from the initial S-wave couplings. Although these corrections are rather small, their interferences with the tree-level amplitudes can still produce some effects on the invariant mass spectra in the final states. In particular, the presence of the TS mechanism within the near-threshold region will change the energy-dependent behavior of the initial state. It suggests that a proper consideration of the vertex corrections as well as the TS mechanism would be necessary for the study of these axial vector mesons in the future partial wave analysis, e.g., in charmonium radiative or hadronic decays at BESIII.

Our analysis is also useful for a better understanding of the nature of $f_1(1420)$, namely, whether it is a genuine state or just a TS enhancement produced by the $f_1(1285)$ decays. Our study in Ref. [23] and herein suggests that the exclusive TS contributions from $f_1(1285)$ is insufficient for describing the $f_1(1420)$ peak in the $K\bar{K}\pi$ channel, although the line shape is agreeable. The data [30–33] actually call for a pole contribution around 1.42 GeV. This indicates that $f_1(1285)$ and $f_1(1420)$ can still be accommodated by the quark model light axial vector nonet. Meanwhile, the strong $K^*\bar{K}$ final state interactions are strongly entangled with the quark model states. Further experimental evidence and theoretical studies are needed to set up a more consistent picture for the light axial vector nonet in the future.

ACKNOWLEDGMENTS

This work is supported, in part, by the National Natural Science Foundation of China (Grant No. 11521505), the DFG and NSFC funds to the Sino-German CRC 110 "Symmetries and the Emergence of Structure in QCD" (NSFC Grant No. 12070131001, DFG Project-ID No. 196253076), National Key Basic Research Program of China under Contract No. 2020YFA0406300, and Strategic Priority Research Program of Chinese Academy of Sciences (Grant No. XDB34030302).

APPENDIX

We provide the detailed expressions for the transition amplitudes of the triangle loops here. As follows, for brevity we use s_c as an alias for s_{ad}. After contraction, the Lorentz structures of the triangle amplitudes take the following forms:

$$M^{\text{tri}}_{c,d} = -\frac{ig_{c,d}}{s_c - m^2_{K^*} + im_{K^*}\Gamma_{K^*}}\epsilon_\mu[\chi_a(s_0,s_a,s_b,s_c,s_{ab})p^\mu_a + \chi_b(s_0,s_a,s_b,s_c,s_{ab})p^\mu_b + \chi_d(s_0,s_a,s_b,s_c,s_{ab})p^\mu_d], \quad \text{(A1)}$$

$$M^{\text{tri}}_{a,b} = -\frac{ig_{a,b}}{s_{bd} - m^2_{K^*} + im_{K^*}\Gamma_{K^*}}\epsilon_\mu[\chi_b(s_0,s_b,s_a,s_{bd},s_{ab})p^\mu_a + \chi_a(s_0,s_b,s_a,s_{bd},s_{ab})p^\mu_b + \chi_d(s_0,s_b,s_a,s_{bd},s_{ab})p^\mu_d]. \quad \text{(A2)}$$

The scalar functions χ_r ($r = a, b, d$) are linear combinations of $\{\Lambda_0, \Lambda_{cb}, \Lambda_{bb}\}$, i.e.,

$$\begin{aligned}
\chi_a(s_0, s_a, s_b, s_c, s_{ab}) &= \left(-1 + \frac{s_a - s_d}{s_c}\right)\Lambda_0(s_0, s_b, s_c) + \frac{1}{2s_c}[s_0(s_c + s_a - s_d) + s_b(s_c - s_a + s_d) \\
&\quad + s_c(s_a + s_d - s_c - 2s_{ab})]\Lambda_{cb}(s_0, s_b, s_c), \\
\chi_b(s_0, s_a, s_b, s_c, s_{ab}) &= \frac{1}{2s_c}[s_0(s_c + s_a - s_d) + s_b(s_c - s_a + s_d) + s_c(s_a + s_d - s_c - s_{ab})]\Lambda_{bb}(s_0, s_b, s_c), \\
\chi_d(s_0, s_a, s_b, s_c, s_{ab}) &= \left(1 + \frac{s_a - s_d}{s_c}\right)\Lambda_0(s_0, s_b, s_c) + \frac{1}{2s_c}[s_0(s_c + s_a - s_d) + s_b(s_c - s_a + s_d) \\
&\quad + s_c(s_a + s_d - s_c - s_{ab})]\Lambda_{cb}(s_0, s_b, s_c).
\end{aligned} \tag{A3}$$

It can be immediately verified that (by setting Λ_{bb} and Λ_{cb} to be zero), when there is only the $g^{\mu\alpha}$ term in $I^{\mu\alpha}$ (or when other D-wave terms are negligible), the Lorentz structures of Eqs. (A1) and (A2) will recover the tree-level forms of Eqs. (6) and (7). In such a case, the triangle amplitude will have only the S-wave contributions and will not change the distribution pattern of events in the Dalitz plot.

The coefficients Λ_0, Λ_{bb}, and Λ_{bc} are expressed in terms of standard functions of LoopTools, i.e., C_i, C_{ij}, and C_{ijk}.

Their expressions are

$$\Lambda_0 = \frac{i}{8\pi^2 m_1^2}[2s_b\delta C_{001} + (s + s_b - s_c)\delta C_{002}], \tag{A4}$$

$$\Lambda_{cb} = \frac{i}{8\pi^2 m_1^2}[2\delta C_{002} + 2s_b\delta C_{112} + (s + 3s_b - s_c)\delta C_{122} + (s + s_b - s_c)\delta C_{222} + 2s_b\delta C_{12} + (s + s_b - s_c)\delta C_{22}], \tag{A5}$$

$$\begin{aligned}
\Lambda_{bb} &= -\frac{i}{4\pi^2}(C_0 + C_1 + C_2) + \frac{i}{8\pi^2 m_1^2}[2\delta C_{00} + 2s_b\delta C_{11} + (s + 3s_b - s_c)\delta C_{12} + (s + s_b - s_c)\delta C_{22} \\
&\quad + 4\delta C_{001} + 4\delta C_{002} + 2s_b\delta C_{111} + (s + 5s_b - s_c)\delta C_{112} + (2s + 4s_b - 2s_c)\delta C_{122} + (s + s_b - s_c)\delta C_{222}],
\end{aligned} \tag{A6}$$

where the δC_{ij}, δC_{ijk} are defined by

$$\delta C_{ij(ijk)} = C_{ij(ijk)} - C_{ij(ijk)}|_{m_1 \to 0}. \tag{A7}$$

[1] P. A. Zyla *et al.* (Particle Data Group), Prog. Theor. Exp. Phys. **2020**, 083C01 (2020).
[2] R. S. Longacre, Phys. Rev. D **42**, 874 (1990).
[3] M. F. M. Lutz and E. E. Kolomeitsev, Nucl. Phys. **A730**, 392 (2004).
[4] L. Roca, E. Oset, and J. Singh, Phys. Rev. D **72**, 014002 (2005).
[5] M. F. M. Lutz and S. Leupold, Nucl. Phys. **A813**, 96 (2008).
[6] L. S. Geng and E. Oset, Phys. Rev. D **79**, 074009 (2009).
[7] H. Nagahiro, K. Nawa, S. Ozaki, D. Jido, and A. Hosaka, Phys. Rev. D **83**, 111504 (2011).
[8] F. Aceti, J. J. Xie, and E. Oset, Phys. Lett. B **750**, 609 (2015).
[9] V. R. Debastiani, F. Aceti, W. H. Liang, and E. Oset, Phys. Rev. D **95**, 034015 (2017).
[10] F. Divotgey, L. Olbrich, and F. Giacosa, Eur. Phys. J. A **49**, 135 (2013).
[11] Y. Zhou, X. L. Ren, H. X. Chen, and L. S. Geng, Phys. Rev. D **90**, 014020 (2014).
[12] L. S. Geng, X. L. Ren, Y. Zhou, H. X. Chen, and E. Oset, Phys. Rev. D **92**, 014029 (2015).
[13] F. Aceti, J. M. Dias, and E. Oset, Eur. Phys. J. A **51**, 48 (2015).
[14] L. D. Landau, Nucl. Phys. **13**, 181 (1959).
[15] J. J. Wu, X. H. Liu, Q. Zhao, and B. S. Zou, Phys. Rev. Lett. **108**, 081803 (2012).

[16] M. Ablikim *et al.* (BESIII Collaboration), Phys. Rev. Lett. **108**, 182001 (2012).
[17] X. G. Wu, J. J. Wu, Q. Zhao, and B. S. Zou, Phys. Rev. D **87**, 014023 (2013).
[18] F. Aceti, W. H. Liang, E. Oset, J. J. Wu, and B. S. Zou, Phys. Rev. D **86**, 114007 (2012).
[19] N. N. Achasov, A. A. Kozhevnikov, and G. N. Shestakov, Phys. Rev. D **92**, 036003 (2015).
[20] M. C. Du and Q. Zhao, Phys. Rev. D **100**, 036005 (2019).
[21] Y. Cheng and Q. Zhao, Phys. Rev. D **105**, 076023 (2022).
[22] X. H. Liu, M. Oka, and Q. Zhao, Phys. Lett. B **753**, 297 (2016).
[23] M. C. Du and Q. Zhao, Phys. Rev. D **104**, 036008 (2021).
[24] M. Mikhasenko, B. Ketzer, and A. Sarantsev, Phys. Rev. D **91**, 094015 (2015).
[25] F. Aceti, L. R. Dai, and E. Oset, Phys. Rev. D **94**, 096015 (2016).
[26] C. Adolph *et al.* (COMPASS Collaboration), Phys. Rev. Lett. **115**, 082001 (2015).
[27] F. K. Guo, C. Hanhart, U. G. Meißner, Q. Wang, Q. Zhao, and B. S. Zou, Rev. Mod. Phys. **90**, 015004 (2018).
[28] F. K. Guo, X. H. Liu, and S. Sakai, Prog. Part. Nucl. Phys. **112**, 103757 (2020).
[29] D. Barberis *et al.* (WA102 Collaboration), Phys. Lett. B **440**, 225 (1998).
[30] T. A. Armstrong *et al.* (Athens-Bari-Birmingham-CERN Collaboration), Phys. Lett. B **146**, 273 (1984).
[31] T. A. Armstrong *et al.* (WA76 Collaboration), Phys. Lett. B **221**, 216 (1989).
[32] D. Barberis *et al.* (WA102 Collaboration), Phys. Lett. B **413**, 225 (1997).
[33] J. Abdallah *et al.* (DELPHI Collaboration), Phys. Lett. B **569**, 129 (2003).
[34] H. J. Jing, S. Sakai, F. K. Guo, and B. S. Zou, Phys. Rev. D **100**, 114010 (2019).